



Determination of prognostic predictors in patients with solitary hepatocellular carcinoma: histogram analysis of multiparametric MRI

Leyao Wang¹ · Rong Cong¹ · Zhaowei Chen¹ · Dengfeng Li¹ · Bing Feng¹ · Meng Liang¹ · Sicong Wang² · Xiaohong Ma¹ · Xinming Zhao¹

Received: 27 May 2023 / Revised: 20 July 2023 / Accepted: 24 July 2023 / Published online: 10 August 2023
© The Author(s), under exclusive licence to Springer Science+Business Media, LLC, part of Springer Nature 2023

Abstract

Purpose To evaluate the histogram parameters of preoperative multiparametric magnetic resonance imaging (MRI) and clinical-radiological (CR) characteristics as prognostic predictors in patients with solitary hepatocellular carcinoma ≤ 5 cm and to determine the optimal time window for histogram analysis.

Methods We retrospectively included 151 patients who underwent preoperative MRI between January 2012 and December 2017. All patients were randomly separated into training and validation cohorts ($n = 105$ and 46). Eight whole-lesion histogram parameters were extracted from T2-weighted images, apparent diffusion coefficient maps, and dynamic contrast-enhanced images. Univariate and multivariate logistic regression analyses were performed to evaluate these histogram parameters and CR variables related to early recurrence (ER) and recurrence-free survival. A nomogram was derived from the clinical-radiological-histogram (CRH) model that incorporated these risk factors. Kaplan–Meier survival analysis was performed to evaluate the prognostic performance of the CRH model.

Results In total, 151 patients (male: female, 130: 21; median age, 54.46 ± 9.09 years) were evaluated. Multivariate logistic regression analysis revealed that the significant risk factors of ER were Mean Absolute Deviation and Minimum in the histogram analysis of the delayed phase images, as well as three important CR variables: albumin-bilirubin grade, microvascular invasion, and tumor size. The nomogram built by incorporating these risk factors showed satisfactory predictive ability in the training and validation cohorts with AUC values of 0.747 and 0.765, respectively. Furthermore, the prognostic nomogram can effectively classify patients into high- and low-risk groups ($p < 0.05$).

Conclusion Multiparametric MRI-derived histogram parameters provide additional value in predicting patient prognosis. The CRH model may be a useful and noninvasive method for achieving prognostic stratification and personalized disease management.

Keywords Hepatocellular carcinoma · Magnetic resonance imaging · Early recurrence · Recurrence-free survival · Nomogram

Leyao Wang, Rong Cong and Zhaowei Chen have contributed equally to this work.

Xiaohong Ma and Xinming Zhao have contributed equally to this work.

✉ Xiaohong Ma
maxiaohong@cicams.ac.cn

✉ Xinming Zhao
zhaoxinming@cicams.ac.cn

¹ Department of Diagnostic Radiology, National Cancer Center/National Clinical Research Center for Cancer/Cancer Hospital, Chinese Academy of Medical Sciences and Peking Union Medical College, Beijing 100021, China

Abbreviations

ADC	Apparent diffusion coefficient
ALBI	Albumin-bilirubin
APHE	Arterial phase hyperenhancement
AP	Arterial phase
AUC	Area under the curve
CI	Confidence interval

² Magnetic Resonance Imaging Research, General Electric Healthcare (China), Beijing 100176, China

CR	Clinical-radiological
CRH	Clinical-radiological-histogram
DP	Delayed phase
DWI	Diffusion-weighted imaging
ER	Early recurrence
HCC	Hepatocellular carcinoma
ICC	Interclass correlation coefficient
LI-RADS	Liver imaging reporting and data system
MAD	Mean absolute deviation
MRI	Magnetic resonance imaging
MVI	Microvascular invasion
OR	Odds ratio
PVP	Portal venous phase
ROC	Receiver operating characteristic
RFS	Recurrence-free survival
VOI	Volume of interest

Introduction

Hepatectomy is the optimal and most acceptable treatment strategy for patients with early-stage hepatocellular carcinoma (HCC), especially for patients with good liver function and solitary tumor less than 5 cm [1, 2]. However, the prognosis of patients with HCC remains unsatisfactory, with approximately 50–70% of patients with HCC relapsing within 5 years after hepatectomy [3, 4]. Early recurrence (ER), which often refers to recurrence or metastasis occurring within 2 years after operation, accounts for approximately 70% of the overall postoperative recurrence rate [1, 5, 6]. The clonal origin of the early recurrent tumors is analogous to that of preoperative primary tumors and is assumed to be the result of latent primary tumor metastasis [7, 8]. Thus, investigation of potential prognostic biomarkers associated with ER is critical, as these could help clinicians identify patients at high risk of recurrence and thus facilitate the implementation of individualized treatment.

Multiparametric magnetic resonance imaging (MRI) is the ideal technique for detecting and diagnosing HCC because of its excellent soft tissue contrast. Multiple investigations have shown a connection between prognosis and preoperative MRI characteristics in patients with HCC [9–11]. Notably, HCC is a complex neoplastic lesion that develops from the multistep carcinogenesis of cirrhotic nodules, during which the blood supply is dramatically altered [12]; and the greater the heterogeneity of the tumor, the more aggressive it is and the worse the prognosis [13].

Histogram analysis is an emerging measurement method that provides accurate information about the tumor microenvironment and heterogeneity, allowing for the extraction of more objective quantitative data from medical images that cannot be determined from the simple visual assessment of MRI characteristics [14, 15]. Histogram parameters,

known as first-order features, are utilized to evaluate the distribution of voxel intensity in tumor tissues. Compared with higher-order radiomics features, histogram parameters have the advantages of simplicity and high reproducibility. However, the predictive ability of histogram analysis for HCC prognosis and the optimal time window for analysis remain unclear.

The main objective of this study was to evaluate histogram parameters and clinical-radiological (CR) characteristics as prognostic predictors in patients with solitary HCC ≤ 5 cm and to determine the optimal time window for histogram analysis.

Methods

This retrospective single-center study was approved by the Institutional Review Board, and the requirement for informed consent was waived owing to the retrospective study design.

Study participants

Between January 2012 and December 2017, 1462 patients with HCC who underwent preoperative MRI and surgical resection in our hospital were recruited. The current study included patients who met the following criteria: (a) had single HCC ≤ 5 cm, (b) no preoperative tumor-related treatments before curative resection, (c) good MRI quality for analysis, (d) complete follow-up data and clinical information, and (e) no history of other malignancies. The exclusion criteria were as follows: (a) multiple tumors or single tumor > 5 cm, (b) preoperative tumor-related treatment, (c) unavailable clinical-pathological information or loss to follow-up, and (d) history of other malignancies. Thus, our final study population comprised 151 patients with HCC (130 males and 21 females; median age, 54.46 ± 9.09 years; age range, 27–80 years) (Fig. 1). The clinical variables and laboratory indices involved in the study were age, sex, hepatitis status, cirrhosis, serum alpha-fetoprotein level, alanine transaminase, aspartate aminotransferase, gamma-glutamyl transpeptidase, alkaline phosphatase, total bilirubin, and direct bilirubin. The albumin-bilirubin (ALBI) grade was calculated as previously described [16]. Pathological information was collected from pathological reports, including the Edmondson-Steiner grade and microvascular invasion (MVI) status.

MRI protocol

All patients underwent preoperative multiparametric MRI examination using two 3.0-T scanners (Discovery MR 750 and Signa HDx, GE Medical Systems). The baseline

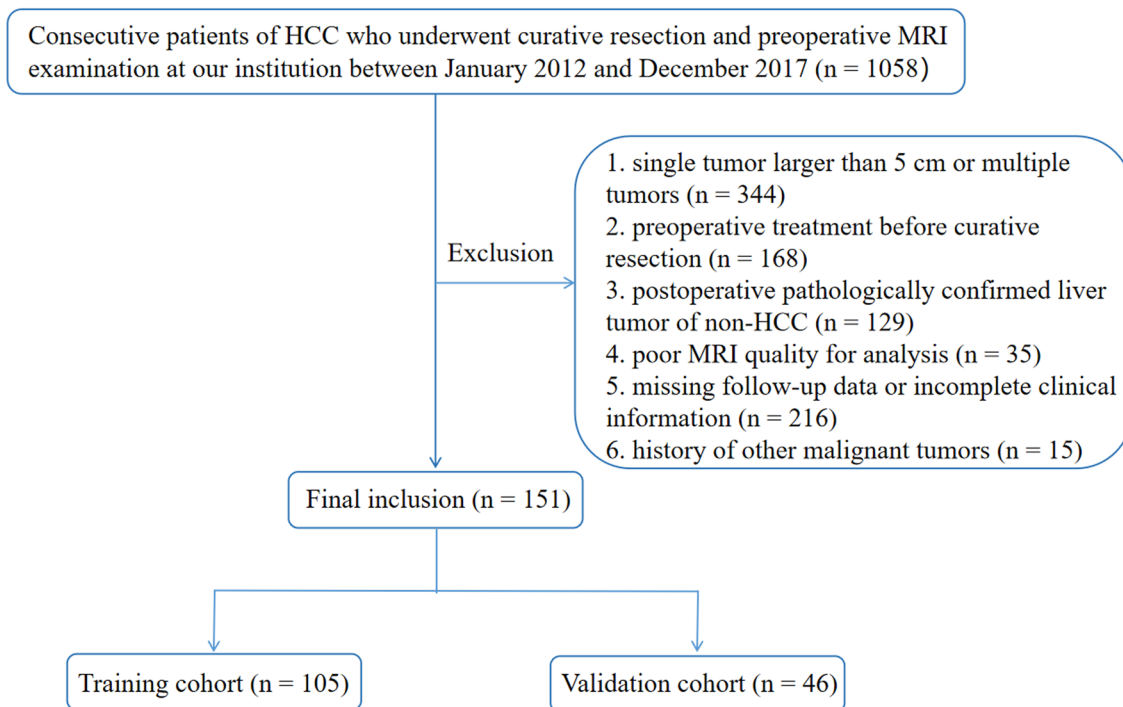


Fig. 1 Flow chart of patient enrollment

sequences consisted of in-phase and opposed-phase axial T1-weighted images, axial fat-suppressed T2-weighted images (T2WI-FS), diffusion-weighted images (DWI, b values = 0 and 800 s/mm²), and fat-suppressed T1-weighted dynamic contrast-enhanced images. Apparent diffusion coefficient (ADC) maps were generated from the DWI images using the function tool ADC software. At 20–25 s (arterial phase, AP), 60–70 s (portal venous phase, PVP), and 100–120 s (delayed phase, DP) after injection of contrast agent, dynamic contrast-enhanced MRI was acquired using a three-dimensional spoiled gradient echo liver acceleration volume acquisition sequence. For dynamic

contrast-enhanced images, 0.2 mL/kg of gadoteric acid (Omniscan 0.5 mmol/mL; GE Healthcare) was injected via an autoinjector at 2.0 mL/s and followed by 20 mL saline flush. Detailed acquisition information is presented in Table 1.

Qualitative and quantitative analyses

Two abdominal radiologists (with 5 years and 9 years of abdominal MRI experience) performed a retrospective review of all imaging features. Both radiologists were blinded to patient information and prognosis. When

Table 1 MRI parameters

	Sequence	TR (ms)	TE (ms)	FOV (cm)	Bandwidth (kHz)	Slice Thickness (mm)	Gap (mm)	Acquisition matrix (phase × frequency)	NEX
GE Signa HDx	Dual-echo T1WI	4.6	2.5/1.3	40.0 × 32.0	142.9	5.0	− 2.5	256.0 × 224.0	0.7
	T2WI/FS	10000.0	91.9	36.0 × 36.0	62.5	6.0	1.0	320.0 × 320.0	2.1
	DWI	8571	59.3	36.0 × 36.0	250.0	6.0	1.0	128.0 × 128.0	2.0
	LAVA	3.9	1.6	36.0 × 28.8	100.0	4.8	− 2.4	288.0 × 192.0	0.7
GE Discovery 750	Dual-echo T1WI	3.9	2.2/1.2	36.0 × 28.8	200.0	5.0	− 2.5	256.0 × 224.0	0.7
	T2WI/FS	6000.0	85.6	38.0 × 30.4	83.3	6.5	1.0	320.0 × 224.0	4.0
	DWI	6316	58.8	38.0 × 30.4	250.0	6.5	1.0	128.0 × 160.0	2.0
	LAVA	3.1	1.3	36.0 × 28.8	125.0	5.0	− 2.5	256.0 × 192.0	0.7

TR repetition time, TE echo time, FOV field of view, NEX number of excitations, T1WI T1-weighted imaging, T2WI T2-weighted imaging, FS fat suppression, DWI diffusion-weighted imaging, LAVA liver acquisition with volume acceleration

there was a disagreement between the two evaluators, a third, more senior radiologist (with 20 years of abdominal MRI experience) was consulted, and an agreement was reached. The following imaging characteristics were analyzed in accordance with the Liver Imaging Reporting and Data System (LI-RADS) version 2018: non-rim arterial phase hyperenhancement (APHE), non-peripheral wash-out, enhancing capsule, mosaic architecture, fat in mass, blood products in mass, corona enhancement, restricted diffusion, and mild-moderate T2 hyperintensity. Tumor size was defined as the maximum tumor diameter measured on transverse or coronal images. Two non-LI-RADS imaging features, non-smooth tumor margin and incomplete tumor capsule, were also analyzed.

Tumor segmentation and parameters extraction

One radiologist (with 5 years of experience in abdominal radiology) manually drew the volumes of interest (VOI) along the tumor boundary on T2WI-FS images, ADC maps, and dynamic contrast-enhanced images (including AP, PVP, and DP images) using the ITK-SNAP software (v.3.8.0; www.itksnap.org, open-source software) (Supplementary Figure 1). Another radiologist (with 9 years of experience in abdominal radiology) independently segmented the VOI of all lesions to assess the interclass correlation coefficient (ICC). Following VOI segmentation, histogram parameters consisted of (a) Skewness, (b) Entropy, (c) Maximum, (d) Mean Absolute Deviation (MAD), (e) Minimum, (f) Uniformity, (g) Variance, and (h) Kurtosis were extracted from each sequence using the Artificial Intelligence Kit software (version 3.3.0, GE Healthcare) based on the open source Pyradiomics Python package.

Follow-up surveillance

All patients underwent routine postoperative follow-up every 3–6 months in the first 2 years and at least once a year thereafter, including serum alpha-fetoprotein tests and imaging (ultrasound, enhanced computed tomography, or MRI). ER was defined as the occurrence of typical imaging features of intra/extrahepatic recurrence or pathologically confirmed metastases within 2 years after surgery. Recurrence-free survival (RFS) was defined as the period between the date of curative resection and the date of recurrence or the last follow-up. All the patients were monitored until June 2022.

Statistical analysis

Data in accordance with normal distribution were expressed as mean \pm standard deviation and compared using an independent samples t-test. Data in accordance with skewed distribution were expressed as medians and compared using the

Mann–Whitney U test. The clinical characteristics and imaging features with p values < 0.1 in the univariate analysis were then incorporated into the multivariate logistic regression analysis to identify significant independent predictors of ER. Only stable features with ICCs over 0.75 were kept. The diagnostic performance of the different models was evaluated using the corresponding area under the receiver operating characteristic (ROC) curve (AUC), accuracy, sensitivity, and specificity. The RFS rates between the low- and high-risk groups were assessed using Kaplan–Meier survival curves with log-rank tests. Two-tailed p values < 0.05 were considered statistically significant. Statistical analyses were performed using SPSS (version 25.0, IBM), R software (version 3.5.1), and Python (version 3.5.6).

Results

Patient characteristics

The final cohort comprised 151 patients (130 males and 21 females; median age, 54.46 ± 9.09 years; age range, 27–80 years) with solitary HCC ≤ 5 cm and all patients were randomized allocated to either the training cohort ($n = 105$, 90 males and 15 females) or the validation cohort ($n = 46$, 40 males and 6 females). CR variables did not differ significantly between the training and validation cohorts (all $p > 0.05$), with the exception of corona enhancement ($p = 0.046$). Of the patients included in this study, 54 experienced ER and 85 relapsed at the end of follow-up. In the training cohort, 38 patients experienced ER and 59 patients relapsed at the end of follow-up. In the validation cohort, 16 patients experienced ER and 26 patients relapsed at the end of follow-up. The median RFS was 43.87 months (range, 1.43–119.83 months) in the training cohort and 46.19 months (range, 3.5–114.7 months) in the validation cohort, respectively (Table 2).

Determination of optimal histogram analysis

The ICCs of inter-observer reproducibility for the histogram parameters are listed in the Supplementary Table 1. In the whole population, the scatter plot showed that Kurtosis from the T2WI-FS images, Skewness from the AP images, Entropy, Maximum, MAD, Minimum, Uniformity, and Variance from the histogram analysis of the PVP and DP images were significant risk factors for ER (Fig. 2). In particular, the histogram parameters from the analysis of the PVP and DP images had the greatest and similar impacts. In the training cohort, univariate analysis showed that the histogram parameters that significantly correlated with ER were Entropy, Maximum, MAD, Minimum, Uniformity, and Variance from the PVP and DP images. Multivariate

Table 2 Baseline characteristics of patients in the training and validation cohorts

Characteristic	Total	Training cohort (n = 144)	Validation cohort (n = 63)	p value
Age (years), mean ± SD	54.46 ± 9.09	54.18 ± 9.39	55.09 ± 8.41	0.575
Sex (male/female)	130/21 (86.09%/13.91%)	90/15 (85.71%/14.29%)	40/6 (86.96%/13.04%)	0.839
Hepatitis (HBV/HCV/ HBV+HCV/none)	130/8/5/8 (86.09%/5.30%/3.31%/5.30%)	88/7/4/6 (83.81%/6.67%/3.81%/5.71%)	42/1/1/2 (91.30%/2.17%/2.17%/4.35%)	0.784
AFP (ng/ml) (≤ 20/20–400/≥ 400)	79/42/30 (52.32%/27.81%/19.87%)	51/30/24 (48.57%/28.57%/22.86%)	28/12/6 (60.87%/26.09%/13.04%)	0.280
ALT (U/L) (> 50/≤ 50 U/L)	17/134 (11.26%/88.74%)	12/93 (11.43%/88.57%)	5/41 (10.87%/89.13%)	0.920
AST (U/L) (> 40/≤ 40 U/L)	19/132 (12.58%/87.42%)	14/91 (13.33%/86.67%)	5/41 (10.87%/89.13%)	0.674
GGT (U/L) (> 60/≤ 60 U/L)	34/117 (22.52%/77.48%)	24/81 (22.86%/77.14%)	10/36 (21.74%/78.26%)	0.880
ALP (U/L) (> 125/≤ 125 U/L)	5/146 (3.31%/96.69%)	4/101 (3.81%/96.19%)	1/45 (2.17%/97.83%)	0.982
TBIL (umol/L) (> 26/≤ 26 umol/L)	4/147 (2.65%/97.35%)	3/102 (2.86%/97.14%)	1/45 (2.17%/97.83%)	0.757
DBIL (umol/L) (> 4/≤ 4 umol/L)	90/61 (59.60%/40.40%)	62/43 (59.05%/40.95%)	28/18 (60.87%/39.13%)	0.834
ALBI grade (1/2/3)	132/19/0 (87.42%/12.58%/0%)	92/13/0 (87.62%/12.38%/0%)	40/6/0 (86.96%/13.04%/0%)	0.910
ES grading (I/II/III)	7/101/43 (4.64%/66.89%/28.48%)	5/69/31 (4.76%/65.71%/29.52%)	2/32/12 (4.35%/69.57%/26.09%)	0.902
MVI (present/absent)	45/106 (29.80%/70.20%)	32/73 (30.48%/69.52%)	13/33 (28.26%/71.74%)	0.784
Cirrhosis (present/absent)	80/71 (52.98%/47.02%)	61/44 (58.10%/41.90%)	27/19 (58.70%/41.30%)	0.057
Non-rim APHE (present/absent)	127/24 (84.11%/15.89%)	87/18 (82.86%/17.14%)	40/6 (86.96%/13.04%)	0.526
Non-peripheral washout (present/absent)	120/31 (79.47%/20.53%)	83/22 (79.05%/20.95%)	37/9 (80.43%/19.57%)	0.846
Enhancing capsule (present/absent)	128/23 (84.77%/15.23%)	88/17 (83.81%/16.19%)	40/6 (86.96%/13.04%)	0.620
Tumor size (cm)	3.48 (2.70, 4.30)	3.45 (2.60, 4.00)	3.50 (2.70, 4.63)	0.307
Mosaic architecture (present/absent)	41/110 (27.15%/72.85%)	27/78 (25.71%/74.29%)	14/32 (30.43%/69.57%)	0.548
Fat in mass (present/absent)	24/127 (15.89%/84.11%)	18/87 (17.14%/82.86%)	6/40 (13.04%/86.96%)	0.526
Blood products in mass (present/absent)	24/127 (15.89%/84.11%)	19/86 (18.10%/81.90%)	5/41 (10.87%/89.13%)	0.264
Corona enhancement (present/absent)	31/120 (20.53%/79.47%)	17/88 (16.19%/83.81%)	14/32 (30.43%/69.57%)	0.046
Mild-moderate T2 hyperintensity (present/absent)	136/15 (90.07%/9.93%)	93/12 (88.57%/11.43%)	43/3 (93.48%/6.52%)	0.527
Restricted diffusion (present/absent)	142/9 (94.04%/5.96%)	99/6 (94.29%/5.71%)	43/3 (93.48%/6.52%)	0.857
Incomplete tumor capsule (present/absent)	65/86 (43.05%/56.95%)	42/63 (40.00%/60.00%)	23/23 (50.00%/50.00%)	0.253
Non-smooth tumor margin (present/absent)	75/76 (49.67%/50.33%)	51/54 (48.57%/51.43%)	24/22 (52.17%/47.83%)	0.684

SD Standard deviation, HBV Hepatitis B virus, HCV Hepatitis C virus, AFP Alpha-fetoprotein, ALT Alanine transaminase, AST Aspartate aminotransferase, GGT Gamma-glutamyl transpeptidase, ALP Alkaline phosphatase, TBIL Total bilirubin, DBIL Direct bilirubin, ALBI Albumin-bilirubin, ES Edmondson-Steiner, MVI microvascular invasion, APHE Arterial phase hyperenhancement

logistic regression revealed two parameters, MAD ($p = 0.002$, odds ratio [OR] 0.776, 95% confidence interval [CI] 0.288–1.265) and Minimum ($p = 0.061$, OR – 0.425, 95% CI – 0.869–0.020) from the DP images, which were significantly associated with ER. The optimal cut-off values for MAD and Minimum were 7.421 and 6.782, respectively. The AUC, accuracy, sensitivity, and specificity of the histogram model for predicting ER were 0.716 (95% CI 0.635–0.795),

0.619, 94.7%, and 43.3% in the training cohort, and 0.694 (95% CI 0.560–0.819), 0.630, 81.2%, and 53.3% in the validation cohort, respectively (Fig. 3A and B).

CR model construction

Univariate analysis showed that the CR variables for ER were ALBI grade ($p = 0.003$), tumor size ($p = 0.097$), MVI

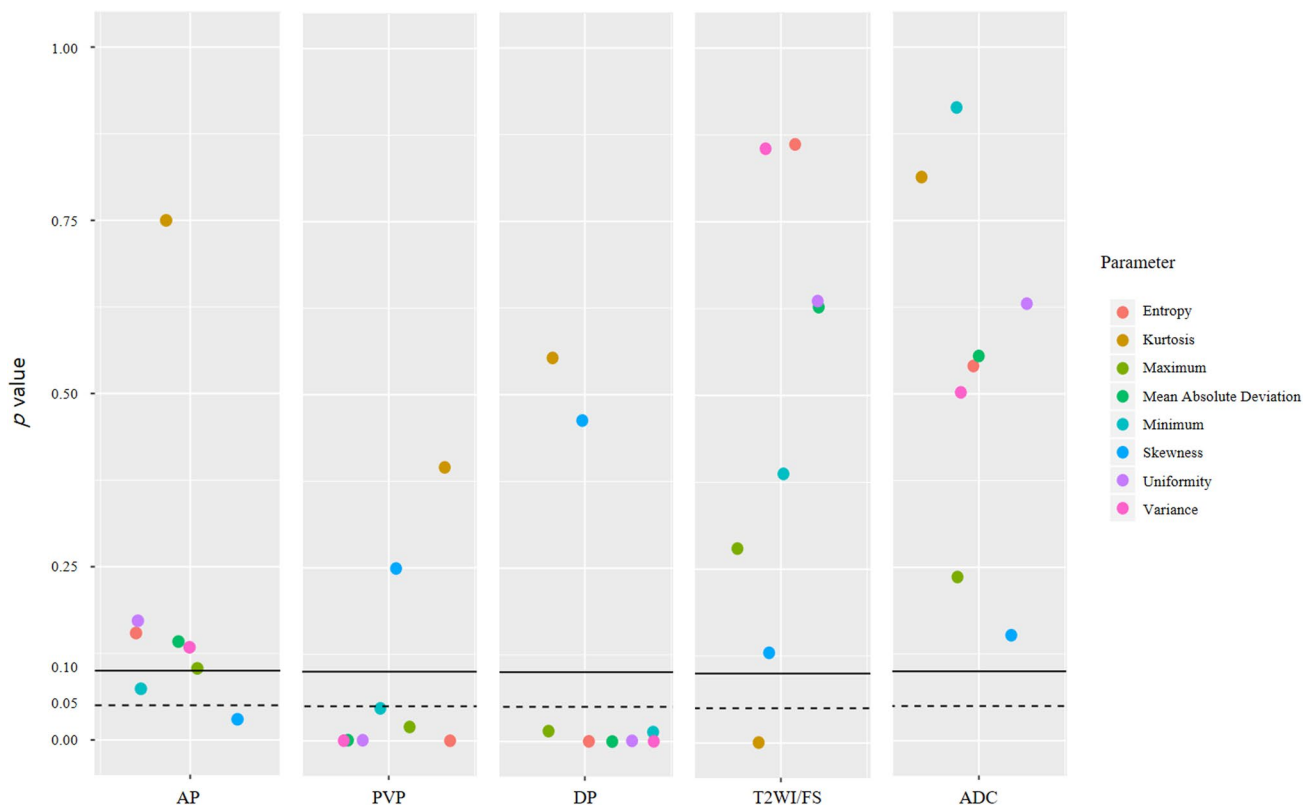


Fig. 2 Scatter plot represents the effect of histogram parameters of different sequences on the prognosis of patients in the univariate analysis

($p = 0.029$), age ($p = 0.014$), non-rim APHE ($p = 0.066$), and alanine transaminase levels ($p = 0.056$). Multivariate logistic regression analysis revealed that the independent risk variables related to ER were ALBI grade ($p = 0.040$, OR 4.018, 95% CI 1.064–15.177), MVI ($p = 0.068$, OR 2.334, 95% CI 0.940–5.791), and tumor size ($p = 0.026$, OR 1.622, 95% CI 1.059–2.484) (Table 3). The AUC, accuracy, sensitivity, and specificity of the CR model for predicting ER were 0.690 (95% CI 0.594–0.791), 0.714, 44.7%, and 86.6% in the training cohort, and 0.666 (95% CI 0.514–0.804), 0.696, 43.8%, and 83.3% in the validation cohort, respectively (Fig. 3C and D).

Prognostic potential of the CRH model

The final CRH model that predicted ER for HCC included MAD and Minimum from the histogram analysis of the DP images, ALBI grade, MVI, and tumor size. For ER prediction, the AUC, accuracy, sensitivity, and specificity of the CRH model were 0.747 (95% CI 0.664–0.827), 0.667, 76.3%, and 61.2% in the training cohort and 0.765 (95% CI 0.641–0.871), 0.630, 62.5%, and 63.3% in the validation cohort, respectively (Table 4). The ROC curves of the CRH model in the training and validation cohorts are shown in

Fig. 3E and F. The nomogram and calibration curves for the CRH model are shown in Fig. 4.

Using a critical value of 0.336, the training cohort was classified into high- and low-risk groups for RFS prediction. The RFS rate was significantly higher in the low-risk group than in the high-risk group, as confirmed in the validation cohort (training cohort, $p < 0.001$; validation cohort, $p = 0.002$) (Fig. 5).

Discussion

Our results revealed that histogram parameters, including MAD and Minimum from the histogram analysis of DP images, were the most valuable predictors of ER and poor RFS in patients with solitary HCC ≤ 5 cm. The prediction nomogram created by integrating optimal histogram parameters and CR risk factors (including ALBI grade, MVI, and tumor size) effectively distinguished patient prognosis.

Artificial intelligence is widely used in both clinical and scientific research. However, compared with complex artificial intelligence models, histogram analysis has the advantages of simplicity and high reproducibility, and eliminates the need for complex post-processing techniques. Several studies have achieved good results in assessing the prognosis

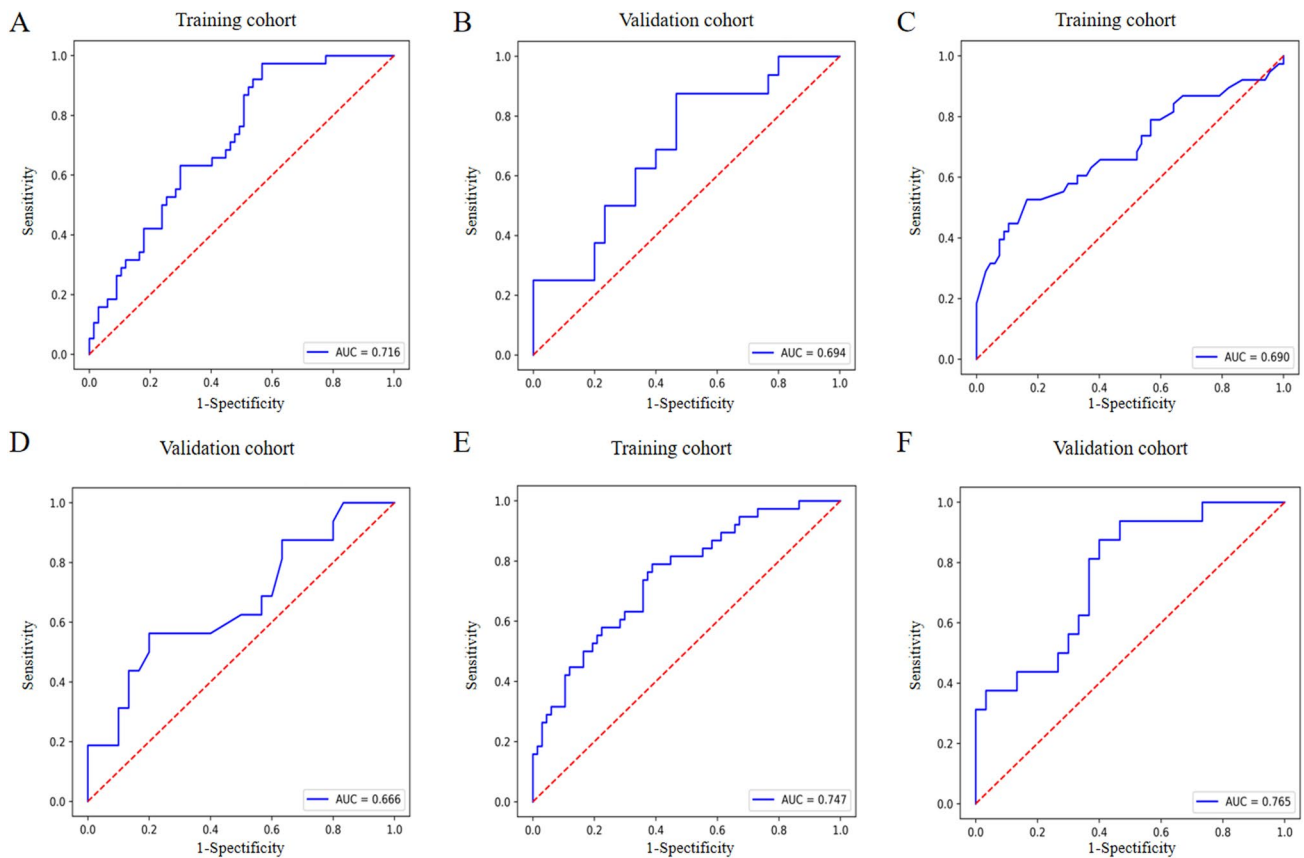


Fig. 3 The distribution and performance of three different models. **A** ROC curve of the histogram model in the training cohort. **B** ROC curve of the histogram model in the validation cohort. **C** ROC curve of the CR model in the training cohort. **D** ROC curve of the

CR model in the validation cohort. **E** ROC curve of the CRH model in the training cohort. **F** ROC curve of the CRH model in the validation cohort. *CR* Clinical-radiological, *CRH* Clinical-radiological-histogram, *ROC* Receiver operator characteristic

of various cancers using MRI-derived histogram analysis [17–19]. Zhang et al. [20] reported that Entropy from the histogram analysis of AP images was the most valuable predictor of ER in patients with HCC. Moreover, the Mean derived from the T1-weighted images and Entropy derived from PVP images were found to be the most effective predictors of MVI [21]. In the present study, we found that MAD and Minimum from the histogram analysis of DP images were independent predictors of ER. The cause of this result may be that the heterogeneity of the HCC in the DP images was more clearly shown and thus contained more tumor heterogeneity information that could be extracted and used to analyze the prognosis of patients. Based on the results of the current study, histogram analysis of DP phase provides prognostic value for patient prognosis, and subsequent studies with larger sample sizes are needed to confirm this conclusion.

Our findings contradict some earlier studies that demonstrated histogram analysis of ADC maps is an important imaging marker for predicting tumor aggressiveness and survival in patients with HCC following curative resection

[22–24]. For instance, Lee et al. [23] and Nakanishi et al. [24] found that the ADC_{min} is a reliable indicator of HCC histological grade and ER prediction. However, the current study indicated that the histogram parameters of ADC maps were not risk factors for ER. One possible explanation for this result may be that different sequences have different predictive values in assessing patient prognosis. DWI is a noninvasive MRI technique that can quantify the diffusion of water molecules in biological tissues, which is reflected in the ADC values. However, the comprehensive and effective heterogeneous characteristics of the tumor can be described more accurately using dynamic contrast-enhanced images than using ADC maps. As a result, in the current multiparametric investigation, the histogram parameters derived from ADC maps were ineffective in predicting the ER.

ALBI grade, a simple and effective biomarker that correlates liver function and survival outcomes based solely on serum total bilirubin and albumin levels, is one of the most commonly used indicators of HCC [16]. Significant differences in ALBI grade occur among patients with different prognoses. In our study, baseline ALBI grade was associated

Table 3 Univariate and multivariate analyses of clinical-radiological variables associated with early recurrence of HCC patients in the training cohort

Variable	Univariate analysis		Multivariate analysis	
	Hazard ratio	<i>p</i> value	Hazard ratio	<i>p</i> value
Sex	1.665 (0.552–5.021)	0.365		
Age	1.060 (1.012–1.110)	0.014		
Hepatitis	1.227 (0.592–2.545)	0.582		
AFP	0.764 (0.454–1.284)	0.310		
ALT	3.556 (0.968–13.070)	0.056		
AST	2.800 (0.822–9.541)	0.100		
GGT	1.580 (0.588–4.246)	0.364		
ALP	0.878 (0.077–10.019)	0.917		
TBIL	1.784 (0.108–29.360)	0.685		
DBIL	0.987 (0.441–2.211)	0.975		
ALBI grade	5.723 (1.832–17.883)	0.003	4.018 (1.064–15.177)	0.040
ES grading	1.031 (0.502–2.120)	0.933		
MVI	2.580 (1.102–6.044)	0.029	2.334 (0.940–5.791)	0.068
Cirrhosis	1.766 (0.782–3.989)	0.171		
Tumor size	1.380 (0.943–2.019)	0.097	1.622 (1.059–2.484)	0.026
Non-rim APHE	0.380 (0.135–1.066)	0.066		
Non-peripheral washout	0.674 (0.263–1.730)	0.412		
Enhancing capsule	0.828 (0.270–2.535)	0.740		
Mosaic architecture	1.416 (0.599–3.348)	0.429		
Fat in mass	0.864 (0.272–2.744)	0.804		
Blood products in mass	1.935 (0.623–6.014)	0.254		
Corona enhancement	1.422 (0.537–3.768)	0.478		
Mild-moderate T2 hyperintensity	0.992 (0.271–3.633)	0.990		
Restricted diffusion	0.262 (0.046–1.501)	0.132		
Non-smooth tumor margin	0.672 (0.300–1.507)	0.335		
Incomplete tumor capsule	0.767 (0.340–1.734)	0.524		

ER early recurrence, AFP alpha-fetoprotein, ALT alanine transaminase, AST aspartate aminotransferase, GGT gamma-glutamyl transpeptidase, ALP alkaline phosphatase, TBIL total bilirubin, DBIL direct bilirubin, ALBI albumin-bilirubin, ES edmondson-steiner, MVI microvascular invasion, APHE arterial phase hyperenhancement

Table 4 The AUC, accuracy, sensitivity, and specificity of different models in the validation cohort

	AUC (95% CI)	Accuracy	Sensitivity	Specificity
Clinical-radiological model	0.666 (95% CI 0.514–0.804)	0.696	43.8%	83.3%
Texture model	0.694 (95% CI 0.560–0.819)	0.630	81.2%	53.3%
Combined model	0.765 (95% CI 0.641–0.871)	0.630	62.5%	63.3%

AUC area under the curve, CI confidence interval

with ER and poor RFS, suggesting that baseline liver function could be a good predictor of patient outcomes, which is in accordance with previous studies [25, 26].

As a critical marker of tumor aggressiveness, MVI is a well-established prognostic factor for ER and shorter long-term survival in patients with HCC after curative resection. It is regarded as a crucial pathway for intrahepatic tumor spread and an early indicator of tumor cell dissemination through peritumoral vessels. In the current study, the presence of MVI was strongly associated with postoperative ER

and shorter RFS in patients with single tumor ≤ 5 cm, as previous studies have demonstrated [27–29]. In addition, our results suggested a certain relationship between tumor size and prognosis in patients with HCC. The larger the tumor size, the greater the heterogeneity, which may reflect the underlying poor cell differentiation, necrosis, and tumor angiogenesis.

In addition, the standardized imaging features of LI-RADS version 2018 were evaluated. However, the results of our study showed that preoperative imaging features were

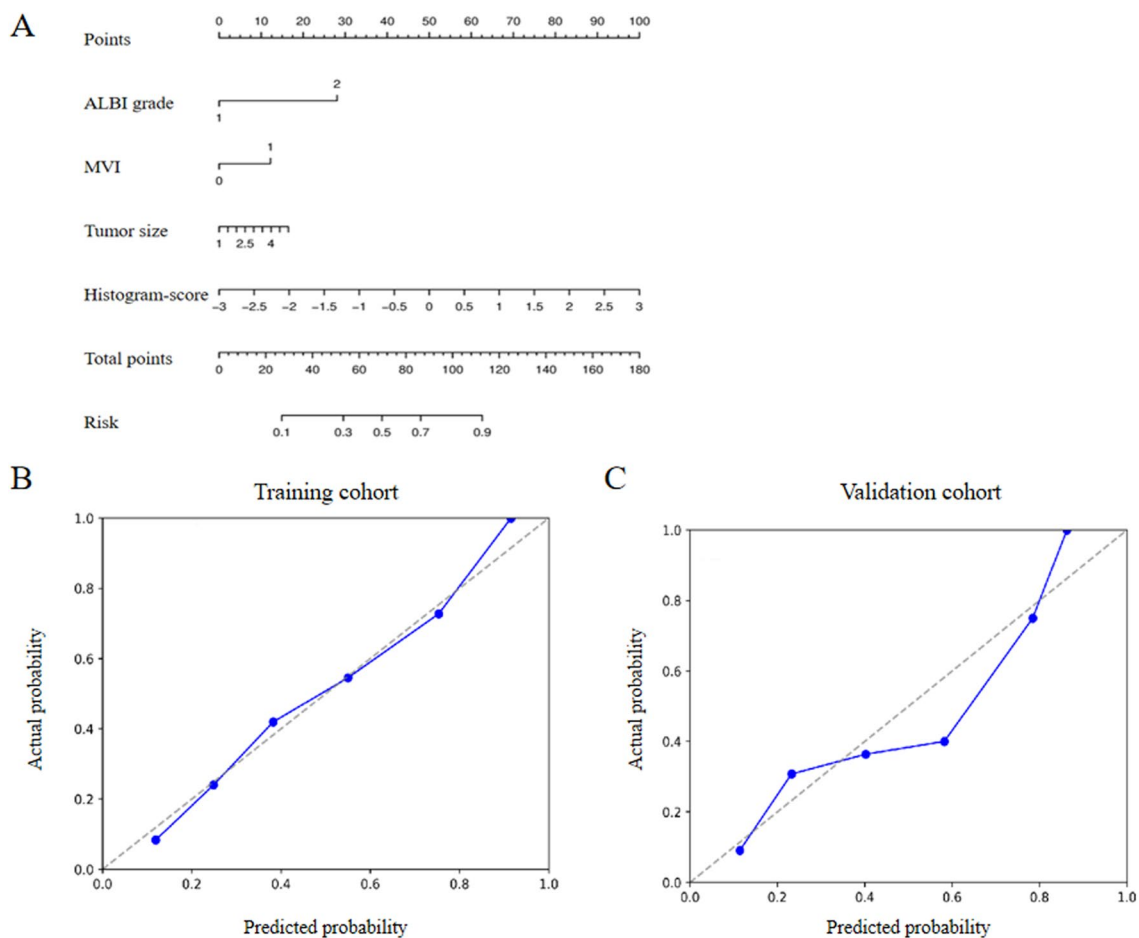


Fig. 4 The nomogram and calibration curves for predicting ER in patients with HCC. **A** The nomogram was developed by combined histogram parameters (Histogram-score), ALBI grade, MVI, and tumor size in the training cohort. **B** Calibration curve of the nomo-

gram in the training cohort. **C** Calibration curve of the nomogram in the validation cohort. *ER* Early recurrence, *HCC* Hepatocellular carcinoma, *ALBI* Albumin-bilirubin, *MVI* Microvascular invasion

not related to the prognosis of patients with HCC. Although the results of the univariate analysis showed that APHE was a prognostic risk factor, it was excluded from the risk factors in the multivariate analysis. A possible reason for this may be that the quantitative analysis of the histogram has a better performance in predicting the prognosis of patients than the imaging features.

This study has several limitations. First, selection bias seems unavoidable, given its retrospective design. Second, the number of patients was relatively small, and were retrospectively enrolled from a single center. Further larger multicenter prospective studies are required to confirm our findings. Third, the findings of this study may not be applicable to MRI imaging using liver-specific contrast agents, and we will conduct quantitative and qualitative analysis of the hepatobiliary phase subsequently. Fourth, the

inclusion and exclusion criteria were strict, and all patients had solitary lesion ≤ 5 cm. Additional studies involving patients with multiple tumors and single tumor > 5 cm in diameter are recommended. Finally, the postoperative follow-up time was insufficient to accurately determine the prognostic predictors of overall survival in patients with HCC. A longer follow-up period is recommended for future studies.

In conclusion, the CRH model constructed by incorporating the MAD and Minimum from the histogram analysis of DP images, ALBI grade, tumor size, and MVI had a significant predictive value for ER and RFS in patients with single HCC ≤ 5 cm. In particular, the DP provided the optimal time window for histogram analysis of the MR images. The prognostic nomogram can effectively stratify the prognostic risk degree and assist clinicians in the surveillance and treatment of patients at high risk of recurrence.

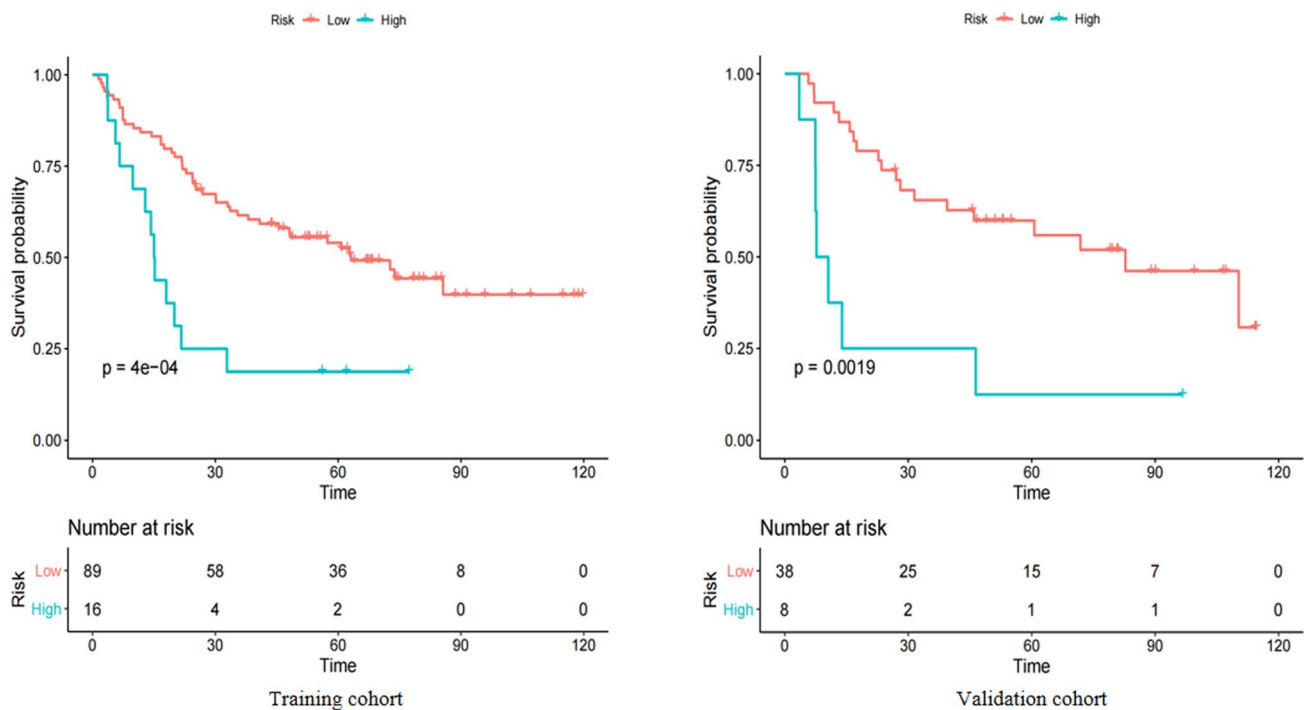


Fig. 5 Kaplan–Meier curves for recurrence-free survival according to the cut-point in the training cohort (left) and validation cohort (right)

Supplementary Information The online version contains supplementary material available at <https://doi.org/10.1007/s00261-023-04015-8>.

Acknowledgements This study is supported by the National Key Research and Development Program of China (No. 2020AAA0109503).

References

- Vilarinho S, Calvisi DF (2014) New advances in precision medicine for hepatocellular carcinoma recurrence prediction and treatment. *Hepatology* 60:1812–1814
- Yang JD, Hainaut P, Gores GJ, Amadou A, Plymoth A, Roberts LR (2019) A global view of hepatocellular carcinoma: trends, risk, prevention and management. *Nat Rev Gastroenterol Hepatol* 16:589–604
- Bruix J, Gores GJ, Mazzaferro V (2014) Hepatocellular carcinoma: clinical frontiers and perspectives. *Gut* 63:844–855
- Forner A, Llovet JM, Bruix J (2012) Hepatocellular carcinoma. *Lancet* 379:1245–1255
- Portolani N, Coniglio A, Ghidoni S et al (2006) Early and late recurrence after liver resection for hepatocellular carcinoma: prognostic and therapeutic implications. *Annals of Surgery* 243:229–235
- Heimbach JK, Kulik LM, Finn RS et al (2018) AASLD guidelines for the treatment of hepatocellular carcinoma. *Hepatology* 67:358–380
- Imamura H, Matsuyama Y, Tanaka E et al (2003) Risk factors contributing to early and late phase intrahepatic recurrence of hepatocellular carcinoma after hepatectomy. *Journal of Hepatology* 38:200–207
- Chen YJ, Yeh SH, Chen JT et al (2000) Chromosomal changes and clonality relationship between primary and recurrent hepatocellular carcinoma. *Gastroenterology* 119:431–440
- An C, Kim DW, Park YN, Chung YE, Rhee H, Kim MJ (2015) Single Hepatocellular Carcinoma: Preoperative MR Imaging to Predict Early Recurrence after Curative Resection. *Radiology* 276:433–443
- Wei H, Jiang H, Zheng T et al (2021) LI-RADS category 5 hepatocellular carcinoma: preoperative gadoxetic acid-enhanced MRI for early recurrence risk stratification after curative resection. *European Radiology* 31:2289–2302
- Ariizumi S, Kitagawa K, Kotera Y et al (2011) A non-smooth tumor margin in the hepatobiliary phase of gadoxetic acid disodium (Gd-EOB-DTPA)-enhanced magnetic resonance imaging predicts microscopic portal vein invasion, intrahepatic metastasis, and early recurrence after hepatectomy in patients with hepatocellular carcinoma. *J Hepatobiliary Pancreat Sci* 18:575–585
- Rimola J (2020) Heterogeneity of Hepatocellular Carcinoma on Imaging. *Seminars in Liver Disease* 40:61–69
- Yang Z, Tang LH, Klimstra DS (2011) Effect of tumor heterogeneity on the assessment of Ki67 labeling index in well-differentiated neuroendocrine tumors metastatic to the liver: implications for prognostic stratification. *American Journal of Surgical Pathology* 35:853–860
- Davnull F, Yip CS, Ljungqvist G et al (2012) Assessment of tumor heterogeneity: an emerging imaging tool for clinical practice? *Insights Imaging* 3:573–589
- Gatenby RA, Grove O, Gillies RJ (2013) Quantitative imaging in cancer evolution and ecology. *Radiology* 269:8–15
- Johnson PJ, Berhane S, Kagebayashi C et al (2015) Assessment of liver function in patients with hepatocellular carcinoma: a new evidence-based approach—the ALBI grade. *Journal of Clinical Oncology* 33:550–558

17. Eun NL, Kang D, Son EJ, Youk JH, Kim JA, Gweon HM (2021) Texture analysis using machine learning-based 3-T magnetic resonance imaging for predicting recurrence in breast cancer patients treated with neoadjuvant chemotherapy. *European Radiology* 31:6916–6928
18. Zhang S, Chiang GC, Magge RS et al (2019) Texture analysis on conventional MRI images accurately predicts early malignant transformation of low-grade gliomas. *European Radiology* 29:2751–2759
19. Baek TW, Kim SH, Park SJ, Park EJ (2020) Texture analysis on bi-parametric MRI for evaluation of aggressiveness in patients with prostate cancer. *Abdom Radiol (NY)* 45:4214–4222
20. Zhang J, Liu X, Zhang H et al (2019) Texture Analysis Based on Preoperative Magnetic Resonance Imaging (MRI) and Conventional MRI Features for Predicting the Early Recurrence of Single Hepatocellular Carcinoma after Hepatectomy. *Academic Radiology* 26:1164–1173
21. Wilson GC, Cannella R, Fiorentini G et al (2020) Texture analysis on preoperative contrast-enhanced magnetic resonance imaging identifies microvascular invasion in hepatocellular carcinoma. *HPB (Oxford)* 22:1622–1630
22. Jing M, Cao Y, Zhang P et al (2021) The Benefit of Apparent Diffusion Coefficient in Evaluating the Invasiveness of Hepatocellular Carcinoma. *Frontiers in Oncology* 11:719480
23. Lee S, Kim SH, Hwang JA, Lee JE, Ha SY (2019) Pre-operative ADC predicts early recurrence of HCC after curative resection. *European Radiology* 29:1003–1012
24. Nakanishi M, Chuma M, Hige S et al (2012) Relationship between diffusion-weighted magnetic resonance imaging and histological tumor grading of hepatocellular carcinoma. *Annals of Surgical Oncology* 19:1302–1309
25. Mao S, Yu X, Shan Y, Fan R, Wu S, Lu C (2021) Albumin-Bilirubin (ALBI) and Monocyte to Lymphocyte Ratio (MLR)-Based Nomogram Model to Predict Tumor Recurrence of AFP-Negative Hepatocellular Carcinoma. *J Hepatocell Carcinoma* 8:1355–1365
26. Lin CY, Lin CC, Wang CC et al (2020) The ALBI Grade is a Good Predictive Model for Very Late Recurrence in Patients with Hepatocellular Carcinoma Undergoing Primary Resection. *World Journal of Surgery* 44:247–257
27. Erstad DJ, Tanabe KK (2019) Prognostic and Therapeutic Implications of Microvascular Invasion in Hepatocellular Carcinoma. *Annals of Surgical Oncology* 26:1474–1493
28. Lee S, Kang TW, Song KD et al (2021) Effect of Microvascular Invasion Risk on Early Recurrence of Hepatocellular Carcinoma After Surgery and Radiofrequency Ablation. *Annals of Surgery* 273:564–571
29. Xu X, Zhang HL, Liu QP et al (2019) Radiomic analysis of contrast-enhanced CT predicts microvascular invasion and outcome in hepatocellular carcinoma. *Journal of Hepatology* 70:1133–1144

Publisher's Note Springer Nature remains neutral with regard to jurisdictional claims in published maps and institutional affiliations.

Springer Nature or its licensor (e.g. a society or other partner) holds exclusive rights to this article under a publishing agreement with the author(s) or other rightsholder(s); author self-archiving of the accepted manuscript version of this article is solely governed by the terms of such publishing agreement and applicable law.